Quenching of Quantum Dot Emission by Fluorescent Gold Clusters: What It Does and Does Not Share with the Förster Formalism

ARTICLE *in* THE JOURNAL OF PHYSICAL CHEMISTRY C · JULY 2013

Impact Factor: 4.77 · DOI: 10.1021/jp404952x

CITATIONS
14

READS
67

3 AUTHORS:

Fadi Aldeek
Florida Department of Agriculture and Cons…
24 PUBLICATIONS **303** CITATIONS
SEE PROFILE

Xin Ji
Florida State University
13 PUBLICATIONS **219** CITATIONS
SEE PROFILE

Hedi Mattoussi
Florida State University
202 PUBLICATIONS **21,783** CITATIONS
SEE PROFILE

THE JOURNAL OF PHYSICAL CHEMISTRY C

Article

pubs.acs.org/JPCC

Quenching of Quantum Dot Emission by Fluorescent Gold Clusters: What It Does and Does Not Share with the Förster Formalism

Fadi Aldeek, Xin Ji, and Hedi Mattoussi*

Department of Chemistry and Biochemistry, Florida State University, 95 Chieftan Way, Tallahassee, Florida 32306, United States

Supporting Information

ABSTRACT: Understanding the interactions that control the energy transfer between dyes, or luminescent quantum dots (QDs), and gold nanoparticles still has several unanswered questions. In this study we probed these interactions using a unique model where CdSe-ZnS QDs were coupled to fluorescent gold nanoclusters (AuNCs). Steady-state and time-resolved fluorescence measurements were used to investigate the effects of spectral overlap and separation distance on the quenching of QD photoemission in these assemblies, using three different size QDs with distinct emission spectra and a variable length polyethylene glycol bridge. We found that the QD photoluminescence quenching efficiency depends on the spectral overlap and separation distance, with larger quenching efficiencies than what would be expected for a QD-dye pair with similar overlap. Moreover, despite the large losses in QD PL, we found no resonance enhancement in the cluster emission for any of the sample configurations used. These results indicate that the mechanism driving the quenching by metal clusters shares an important feature (namely dependence on the spectral overlap) with the Förster dipole−dipole coupling at the heart of fluorescence resonance energy transfer (FRET) and widely validated for dye-dye and QD-dye assemblies. They also prove that the energy losses induced by metal nanostructures are governed by a process that is different from the Förster mechanism.

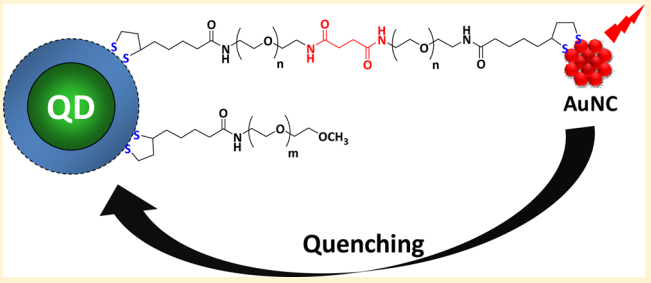

INTRODUCTION

Following the earlier observations proving that proximity to metal surfaces induces strong quenching of dye emission, several reports have shown that gold nanoparticles (AuNPs) as well as other metal nanostructures can act as effective energy quenchers of proximal organic dyes.[1,2] This is in part due to their broad plasmon absorption, which can overlap with the emission spectra of several dye donors and high molar extinction coefficients.[2−4] Such dye−metal nanostructures were further utilized by various groups to develop an array of bioassays including sensing of binding events, oligonucleotide hybridization, and enzymatic activity.[5−9] For instance, Strouse and co-workers have thoroughly investigated the effects of changing the spectral overlap and separation distance on the measured quenching efficiencies for several dye-AuNP pairs.[10]

Energy transfer quenching of luminescent quantum dots (QDs) by AuNPs and redox active complexes has also generated great interest in the past few years.[11−14] Assemblies of QD and metal NPs combine the metal nature of the nanoparticles (namely, broad plasmon absorption and high extinction coefficient) with the narrow and size-tunable emission of the QDs.[15−18] Several groups have shown that the quenching of QD emission in QD-AuNP assemblies, formed using various chemical schemes, strongly depends on the nanoparticle size.[19−22] For example, Song and co-workers compared the quenching efficiencies of CdSe-ZnS QDs coupled to 1.8- and 5-nm AuNPs in vitro and in live cells.[23] In particular, they used polymer-coated QDs, which were modified with sulfo-succinimidyl 4-[*N*-maleimidomethyl]-cyclohexane-1-carboxylate (sulfo-SMCC) heterobifunctional linker, then coupled to a cysteine-terminated peptide; the latter includes a BACE1 (β-secretase 1) cleavage site and C-terminal 6 histidine tag. These QDs were coupled to Ni-nitrilotriacetic acid (Ni-NTA)-modified AuNPs, producing a set of QD-peptide-AuNP assemblies. The authors measured higher quenching efficiencies for assemblies using 5-nm AuNPs compared to those prepared with smaller NPs (1.8 nm). They further used these assemblies to detect enzymatic activity of BACE1 in solution and in cell cultures.

In all these studies, the quenching of dyes or QDs (donors) by proximal AuNPs (acceptors) was found to strongly depend on the separation distance, r, with quenching efficiencies extending beyond the usual threshold imposed by the Förster (fluorescence resonance energy transfer, FRET) dipole−dipole formalism, where donor losses tend to become negligible at $r >$ 10 nm.[24] A few earlier studies have used the Förster mechanism to interpret data collected for dye-metal surfaces, dye-AuNP, and QD-AuNP constructs, where authors have focused on the distance-dependence of the quenching efficiency, with $1/r^6$ dependence reported for ensemble and single molecules

Received: May 20, 2013
Revised: June 24, 2013

   dx.doi.org/10.1021/jp404952x | *J. Phys. Chem. C* XXXX, XXX, XXX−XXX

studies.[11,19] More recently, several studies have suggested that a nanosurface energy transfer (NSET) formalism, based on dipole-surface interactions between the donor and the electron-rich metal surface of AuNPs (with a slower decay of the quenching efficiencies versus separation distance, i.e., $1/r^4$ instead of $1/r^6$), accounts much better for the experimental data.[8,10,25] Furthermore, quenching driven by NSET does not conceptually rely on spectral overlap as FRET does.[25,26]

In a previous report, we investigated the photoluminescence quenching of CdSe-ZnS QDs by 1.4-nm AuNPs using a rigid variable-length polypeptide bridge ($YEHK_m$), made of several core β-strand repeat units, with tyrosine (Y), glutamic acid (E), histidine (H), and lysine (K) residues located at the turns of each unit.[27] In that study we explored the effects of varying the number of AuNPs around a QD and the center-to-center separation distance. We measured higher QD PL quenching efficiencies for those QD-peptide-AuNP conjugates than for their QD-peptide-dye counterparts. We also found that even though the NSET model provided a better description for the observed trend in the distance-dependence of the quenching efficiencies, agreement was only qualitative. The values predicted by the model were consistently smaller than the experimental ones.[27] These findings clearly indicate that overall, the energy transfer process involving Au and potentially other metal NPs requires further work and additional rationales to develop a quantitative understanding of the mechanism(s) involved. Such understanding will also help to design better sensing platforms using AuNP quenchers.

More recently, a few groups have succeeded in developing reproducible synthetic routes to prepare fluorescent gold and silver nanoclusters (AuNCs and AgNCs) with diameters smaller than 2 nm.[28−31] These metal clusters exhibit unique *molecule-like* properties, including broad absorption combined with achievable large Stokes shifts.[30,32,33] In certain instances, tunable emission from green to red and promising colloidal stability have been reported.[31] A few groups have used them in cell labeling studies.[28] We have reported the use of one phase growth along with modular polyethylene glycol (PEG)-functionalized ligands to prepare Au and Ag nanoparticles, and ultrasmall (~1.2 nm) fluorescent clusters with great colloidal stability and broad solubility in aqueous and organic solvents.[15,34,35]

In this report, we probe the interactions of these fluorescing clusters with CdSe-ZnS QDs, using constructs assembled via a polyethylene glycol bridge (i.e., QD-PEG-AuNC conjugates). Three different size QDs (green-, yellow- and red-emitting) and variable length (PEG) ligands have been used to investigate the effects of the spectral overlap and separation distances on the measured quenching efficiencies. Because the metal clusters are fluorescent, our construct provides a new feature to probe the interactions and quenching mechanism involved, namely, by addressing the following question: Is there enhancement in the cluster emission following interaction with the QDs?

EXPERIMENTAL SECTION

Ligand Synthesis. The ligands used in this study are modular in nature; each is made up of a lipoic acid (LA) group appended with a varying length polyethylene glycol (PEG) segment. We used four terminally reactive ligands, LA-PEG_{1000}-NH_2 (PEG M_W = 1000), LA-PEG_{600}-NH_2 (PEG M_W = 600), LA-PEG_{200}-NH_2 (PEG M_W = 200), and LA-PEG_{600}-COOH (PEG M_W = 600), along with one terminally inert ligand, LA-PEG_{750}-OCH_3 (PEG M_W = 750); the latter was used for preparing reference samples and for controlling the fraction of reactive amines per QD. These ligands have been synthesized, purified, and characterized following the protocols detailed in previous reports.[36,37] The chemically-reduced form of the ligands, DHLA-PEG_{750}-OCH_3 mixed with small fractions of DHLA-PEG-NH_2, were applied for cap exchange on the QDs, while pure LA-PEG_{600}-COOH or LA-PEG_{750}-OCH_3 were used for the growth, stabilization, and functionalization of the red-emitting Au clusters.[15,34]

Synthesis and Surface-Functionalization of CdSe-ZnS Quantum Dots. Three different sets of CdSe-ZnS core−shell QDs emitting at 525 nm (green, diameter ≅ 5.6 nm), at 574 nm (yellow, diameter ≅ 6.8 nm), and at 610 nm (red, diameter ≅ 7.8 nm) were prepared and used.[38,39] The QD growth was carried out by reacting organometallic precursors at high temperature in a coordinating solvent mixture made of trioctyl phosphine (TOP), trioctyl phosphine oxide (TOPO), and alkylamines, using two steps: growth of CdSe cores followed by overcoating with 5−6 monolayers of ZnS.[38,40,41] Following growth and purification, cap exchange with a mixture of methoxy-terminated DHLA-PEG_{750} (95%) and amine-terminated DHLA-$PEG_{200/600/1000}$ (5%) has been carried out following the protocols described in our previous reports;[36,37] these QDs are referred to as amine-QDs. We also prepared QDs capped with 100% methoxy-terminated DHLA-PEG_{750} and used them for control experiments.

Growth of Red Fluorescent Gold Nanoclusters (AuNCs). Here, we briefly describe the preparation of COOH-functionalized clusters. In a 50-mL round-bottomed flask, 26.5 mg of LA-PEG_{600}-COOH ligand was dispersed in 20 mL of deionized water, followed by the addition of 50 μL of NaOH (2 M) to maintain the pH at 11. Then, 200 μL of 50 mM $HAuCl_4 \cdot 3H_2O$ was added to the reaction mixture; this corresponds to a Au:ligand molar ratio of 1:3. After 5 min of Au-complexes formation, 400 μL of 50 mM $NaBH_4$ solution was added dropwise. The reaction mixture was further stirred for 15 h at room temperature, and then purified from free ligands and $NaBH_4$ by applying three cycles of centrifugation/filtration, using a membrane filtration device with a molecular weight cutoff of 10 kDa (from Millipore).[34] AuNCs surface-functionalized with LA-PEG_{750}-OCH_3 were prepared and used for control experiments. These clusters are referred to as carboxy (COOH)-AuNCs or methoxy (OMe)-AuNCs.

Covalent Conjugation of Carboxy-AuNCs to Amine-QDs. AuNCs capped with 100% LA-PEG_{600}-COOH (500 μL, 2 μM) were first activated by using 10 000 equiv of EDC (1-ethyl-3-(3-dimethylaminopropyl)carbodiimide) and NHS (*N*-hydroxysuccinimide) in PBS buffer (10 mM, pH 6.5) for 30 min. Excess unreacted EDC and NHS byproducts were removed by centrifugation/filtration, using a membrane filtration device with a cutoff molecular weight of 10 kDa (Millipore). Then, the desired amount of activated AuNCs was added to a dispersion containing 50 μL (from a 2 μM stock dispersion) of amine-QDs in 450 μL of PBS buffer (10 mM, pH 7.4) and incubated for 1 h. The final concentration of QDs in the samples was maintained at 0.2 μM, while the AuNC-to-QD molar ratio was varied between 0-to-1 and 3-to-1. The concentration of AuNCs was calculated by using the extinction coefficient reported for commercially available 1.4 nm size AuNPs (ε_{420} = 112 000 cm^{-1} M^{-1}); the size of the present cluster determined by TEM is ~1.2 nm.[35] This indicates that the extinction coefficient is only approximate, implying that the reported molar ratios are slightly underestimated.[27]

dx.doi.org/10.1021/jp404952x | J. Phys. Chem. C XXXX, XXX, XXX−XXX

Photophysical Characterizations. The optical absorption spectra were collected with use of a UV−vis absorption spectrophotometer, UV 2450 model from Shimadzu (Durham, NC). The emission spectra were collected on a Fluorolog-3 spectrometer (HORIBA Jobin Yvon Inc., Edison, NJ) equipped with TBX PMT and air-cooled CCD camera detectors. The time-resolved (TR) fluorescence decay data were collected and analyzed with a TCSPC (time correlation single photon counting) system integrated into the same Fluorolog-3. We used a pulsed excitation signal at 440 nm (100 ps, fwhm) with a repetition rate of 1 MHz, provided by a NanoLED-440LH, while the detection was collected on the same TBX PMT detector mentioned above. The fluorescence decay traces of the QD emission (limited to a narrow window centered at the peak of the PL spectrum) were fitted to a three-exponential function:

$$I(t) = A_1 e^{-t/\tau_1} + A_2 e^{-t/\tau_2} + A_3 e^{-t/\tau_3} \quad (1)$$

where t is time and A_i is a weighing parameter associated with each decay time, τ_i. From fits of the decay curves using Data Station software (Horiba Jovin-Yvon), we extracted an average amplitude-weighted lifetime defined as:

$$\tau_{avg} = \frac{\sum A_i \tau_i^2}{\sum A_i \tau_i} \quad (2)$$

The PL quenching efficiency, E, was extracted from the steady-state and/or time-resolved fluorescence profiles, using the expressions

$$E = 1 - \frac{F_{DA}}{F_D} \quad (3)$$

for steady-state and

$$E = 1 - \frac{\tau_{DA}}{\tau_D} \quad (4)$$

for time-resolved, where F_{DA} and F_D designate the PL intensity measured for QDs coupled to AuNCs and QDs alone, respectively. Similarly, τ_{DA} and τ_D, designate the exciton lifetime measured for QD-assemblies with and without AuNCs, respectively. The quantum yields of the samples (QY_{sample}) were determined with respect to a reference (QY_{ref}) with use of the following equation: $QY_{sample} = [(F_{sample}/F_{ref})(A_{ref}/A_{sample})(n_{sample}^2/n_{ref}^2)QY_{ref}]$, where F, A, and n are the measured fluorescence (area under the emission peak), absorbance at the excitation wavelength, and the refractive index of the solvent, respectively.[24] The PL QY values were determined relative to Rhodamine 6G in ethanol (QY_{ref} = 94%).

RESULTS AND DISCUSSION

The QD-AuNC assemblies used in this investigation were formed via covalent coupling of luminescent QDs and fluorescent clusters capped with similar PEGylated ligands. The assembly relies on a common and easy to implement coupling strategy, and it provides an inert bridge between the QDs and Au clusters. Starting with carboxy-functionalized clusters (AuNCs grown using LA-PEG_{600}-COOH ligands), the COOH groups were activated with *N*-hydroxysuccinimide (NHS) to yield NHS-activated AuNCs, which were further reacted with amine-functionalized QDs (amine-QDs); the QDs were prepared via cap exchange, using a 95:5 mixture of DHLA-PEG_{750}-OCH_3 (inert) and DHLA-PEG_{600}-NH_2 (reactive) ligands.[36,37] Figure 1A schematically shows a nanoscale construct in which the QD acts as the exciton donor while the clusters are the acceptors/quenchers. These constructs allowed the attachment of controllable numbers of AuNCs to a QD center and the ability to vary the spectral overlap between the AuNC absorption and QD photoluminescence spectra, as well as the separation distance, all via an inert PEG linker. The broad but progressively decaying absorption profile of the clusters expanding to 700 nm allowed easy tuning of the spectral overlap (Figure 2B). We used three different size CdSe-ZnS QDs with emission peaks centered at 525, 574, and 610 nm; these correspond to inorganic core−shell diameters of 5.6, 6.8, and 7.8 nm, respectively (Figure 1B).[41,42] The corresponding spectral overlap integrals, I, were calculated from integration of the spectral overlap function, defined as $J(\lambda) = PL_{D\text{-}corr}(\lambda)\lambda^4\varepsilon_A$, where PL_D and ε_A designate the normalized fluorescence spectrum of the donor and the extinction coefficient spectrum of the acceptor, respectively (see Table 1 and Figure 1B).[43,24]

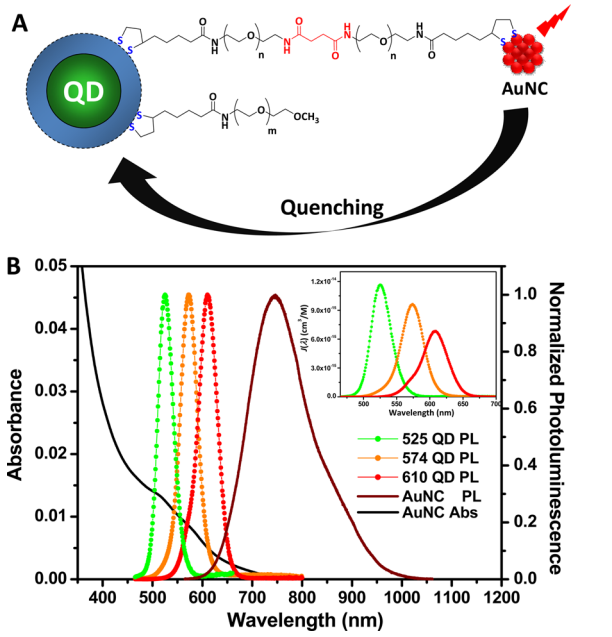

Figure 1. (A) Schematic representation of the QD-PEG-AuNC conjugates; one cluster per conjugate is shown. (B) UV−vis absorption spectrum of AuNCs (black line) and normalized emission spectra of the three CdSe-ZnS QDs used in this study, 525-nm QD (green circle), 574-nm QD (dark yellow circle), and 610-nm QD (red circle) and the far red-emitting AuNCs (red-wine line). The inset shows plots of the resulting overlap functions, $J(\lambda) = PL_{D\text{-}corr}(\lambda)\lambda^4\varepsilon_A(\lambda)$, highlighting the effects of size tuning the QD emission on the degree of spectral overlap with the AuNCs. The absorption spectrum was collected by using a cell with 10 mm optical path and a concentration of 0.2 μM AuNCs.

We would like to stress that the present design differs from what we have used in our previous work.[27] The present quenchers are made of far red-emitting (~750 nm) cluster materials with a size of 1.2 nm, whereas those used previously were made of commercially available (1.4 nm) nonfluorescent small nanoparticles. This provides a new system to test the nature of the interactions between luminescent QDs and metallic platforms beyond the commonly used approach where effects of the separation distance, r, are often investigated. In

dx.doi.org/10.1021/jp404952x | J. Phys. Chem. C XXXX, XXX, XXX−XXX

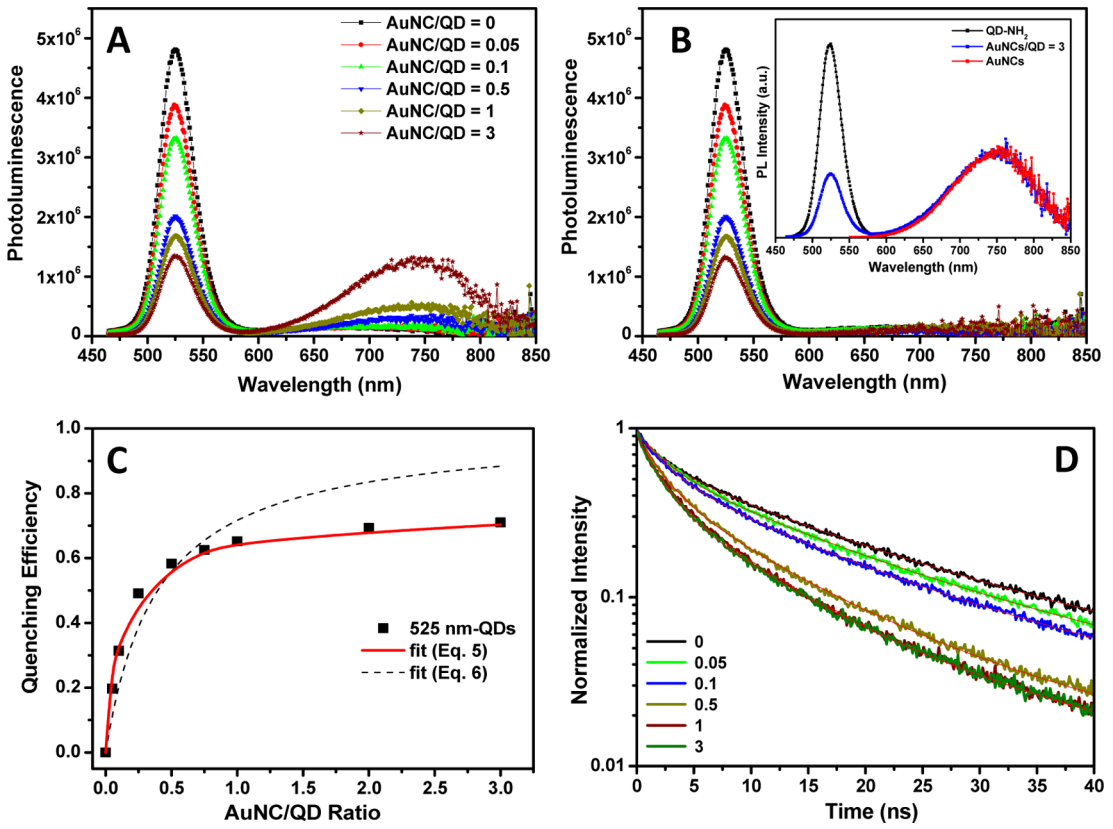

Figure 2. Select PL spectra collected from 525-nm emitting QD-PEG-AuNC conjugates (assembled via a PEG_{600}-plus-PEG_{600} bridge), using excitation at 450 nm, before (A) and after (B) subtracting the contribution from direct excitation of the clusters and signal deconvolution. The inset shows the PL emission spectra of 525-nm QDs, red-emitting AuNCs and QD-PEG-AuNCs conjugates using an AuNC-to-QD ratio of 3-to-1. (C) Plot of the quenching efficiency as a function of the number of AuNCs per QD from data in part B. The quenching data were fitted by using eq 5, accounting for the correction due to conjugate heterogeneity using the Poisson distribution (solid red line) and eq 6 (solid blue line). (D) The corresponding normalized time-resolved PL decay curves with increasing AuNC-to-QD molar ratio. The solid red lines are fits to the data using three-exponential-decay using eq 1, as described in the text.

Table 1. Summary of the Measured PL Quenching Efficiencies for the Three Different Size QDs Used, Together with the Corresponding Spectral Overlap Integrals, and Ratios k_r/k_r^0 and k_{et}/k_r[a]

	525-nm QDs	574-nm QDs	610-nm QDs
PL quenching	0.64 ± 0.019	0.41 ± 0.022	0.17 ± 0.01
overlap integral, $10^{13} \times I$ (cm^3/M)	4.54	4.31	3.46
k_r/k_r^0	0.67 ± 0.026	0.83 ± 0.037	0.97 ± 0.04
k_{et}/k_r	16.21 ± 0.59	5.64 ± 0.49	2.19 ± 0.5

[a]Data compiled for an average QD-AuNC valence of 1.

those studies, authors often focused on addressing the following question: *Does the quenching efficiency vary as the fourth or sixth power of r*?[25,27]

Steady-State and Time-Resolved Fluorescence. We combined steady-state and time-resolved fluorescence measurements to evaluate the QD PL quenching induced by the proximal AuNCs. Figure 2A,B shows the composite and deconvoluted steady-state PL spectra collected from a set of green-emitting (525 nm) QDs, coupled to Au clusters with increasing AuNC-to-QD ratio. The direct excitation contribution to the total signal was removed from the final deconvoluted spectra as shown in Figure 2B. Figure 2C shows a plot of the quenching efficiency, *E*, vs AuNC-to-QD molar ratio extracted from the data. The corresponding time-resolved decay profiles compiled in Figure 2D show a significant decrease in the QD excited-state lifetime upon conjugation to the AuNCs, and that such change also tracks the number of clusters coupled to a QD. The above changes in the steady-state and time-reolved PL clearly show that a pronounced and progressive quenching of the QD PL is measured for increasing AuNC-to-QD ratio. In comparison, control experiments with inert (methoxy-functionalized) AuNCs mixed with amine-QDs or methoxy-terminated QDs mixed with NHS-activated AuNCs show marginal PL quenching, attributable to solution phase interactions (see the Supporting Information, Figure S1). This result indicates that the contributions from nonspecific interactions are negligible.

We have also investigated the effects of varying the spectral overlap between the QD emission and cluster absorption spectra on the measured PL quenching. A representative set of deconvoluted steady-state PL spectra, corrected for direct excitation contribution of the AuNCs, along with time-resolved decay curves collected from the 574-nm-emitting QD-PEG_{600}-plus-PEG_{600}-AuNCs are shown in Figure 3A,B. The data corresponding to 610-nm-emitting QD-AuNC assemblies are shown in the Supporting Information (Figure S2). Figure 3C shows plots of the PL quenching efficiency, *E*, of all three size QDs as a function of the number of AuNCs coupled to (reacted with) the nanocrystals. All these QDs (emitting at 525, 574, and 610 nm) were ligand exchanged with 5% DHLA-PEG_{600}-NH_2 (see the Experimental Section). Data show that

dx.doi.org/10.1021/jp404952x | J. Phys. Chem. C XXXX, XXX, XXX−XXX

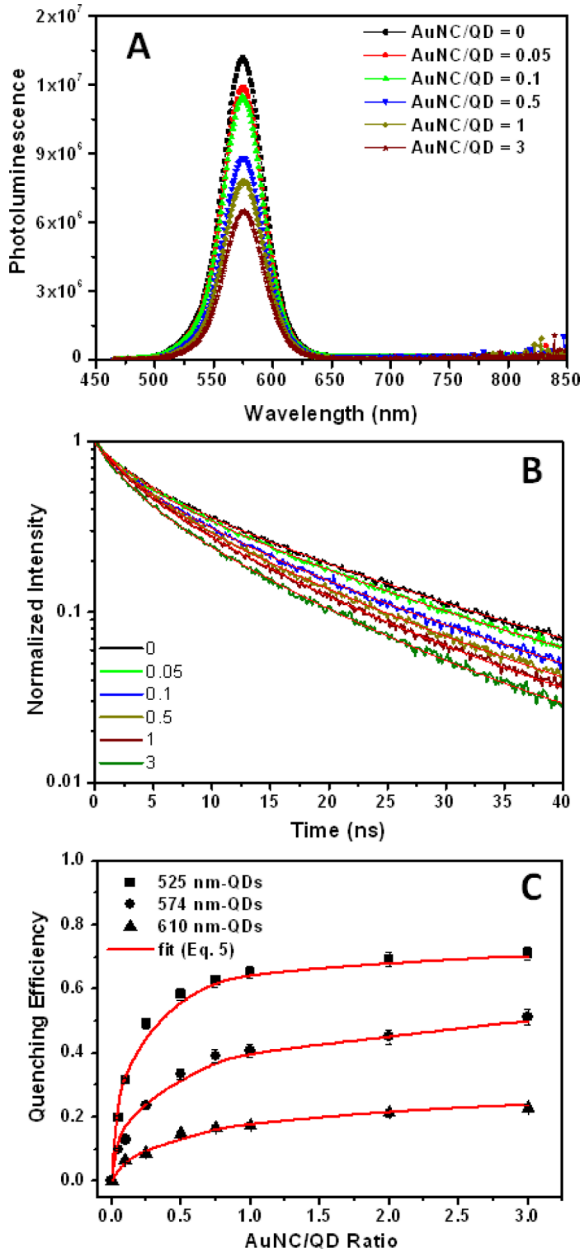

Figure 3. (A) Select PL spectra collected from assemblies using 574-nm-emitting QDs after correction for direct excitation contribution to the cluster emission and signal deconvolution; samples were excited at 450 nm; (B) the corresponding normalized time-resolved PL decay curves with the increasing number of AuNCs per conjugate. (C) Plots of the quenching efficiency versus number of clusters per QD for the three different size QDs, green (square), yellow (circle), and red QDs (triangle) used in this study. The solid red lines correspond to fits to the data using eq 5, as described in the text.

among the dispersions studied, the highest PL quenching is measured for the green-emitting QDs, while the red-emitting QDs experienced the weakest quenching; the green- and red-emitting QDs have the largest and smallest spectral overlap with the cluster absorption, respectively (see Figure 1B). Nonetheless, we should note that in addition to the decrease in the spectral overlap when the QD emission shifts to larger wavelengths (red vs green emission), the center-to-center separation distance is also slightly increased. Though modest, such increase further weakens the interactions and reduces the measured quenching for the yellow- and red-emitting nanocrystals compared to the smaller size (green-emitting) QDs; this occurs in addition to the effects of changes in the spectral overlap.

Finally, we probed the effects of varying the separation distance between QD and AuNCs. This was achieved by using QDs functionalized with different length PEG-amine ligands prior to coupling to the COOH-AuNCs. Three samples of 574-nm (yellow-emitting) QDs were prepared by using 95% DHLA-PEG_{750}-OCH_3 mixed with 5% DHLA-PEG_{200}-NH_2 (M_w = 200), DHLA-PEG_{600}-NH_2 (M_w = 600), or DHLA-PEG_{1000}-NH_2 (M_w = 1000), and conjugated to PEG_{600}-COOH-AuNCs (see the Experimental Section). Figure 4 shows the quenching efficiency measured for these three sets of QD-PEG-bridge-AuNC assemblies. A representative set of deconvoluted spectra, corrected for direct excitation contribution of AuNCs along with time-resolved decay curves collected from QD-AuNC conjugates assembled by using a PEG_{200}-plus-PEG_{600} bridge are also shown. Data collected with use of longer bridges (PEG_{1000}-plus-PEG_{600}) are provided in the Supporting Information (Figure S3). These results clearly indicate that longer PEG bridges (i.e., larger r values) produce smaller quenching efficienies throughout the AuNC-to-QD molar ratios used, and vice versa. The differences measured in the steady-state data are supported by the time-resolved data where shorter exciton lifetimes are measured for the shorter PEG bridge (Figure 4).

We now discuss the above findings within the framework of nonradiative quenching of the QD emission by proximal Au clusters. We attribute the measured and ratio-dependent PL losses for the various QD-PEG-AuNC assemblies to nonradiative loss of the QD excitation energy when Au clusters are brought in close proximity (see Figure 3). Such loss is strongly affected by the degree of spectral overlap and the separation distance, r, as has been observed for QD-dye as well as dye-AuNP pairs.[10,43] The dependence of the quenching efficiency on the AuNC-to-QD ratio (or conjugate valence, n) shown for the various samples (see Figures 3C and 4C) could be best fitted by using an equation of the form:[17]

$$E(N) = \sum_{n=1}^{N} p(n, N)E(n) \tag{5}$$

with $p(n,N) = N^n(e^{-N}/n!)$, where N is the average acceptor-to-QD ratio used and n is the exact number of acceptors (AuNCs) conjugated to the QD. The Poisson distribution function, $p(n,N)$, accounts for heterogeneity in the conjugate valence, and $E(n)$ is given by:[44]

$$E(n) = \frac{\beta n}{\beta n + K} \tag{6}$$

This expression for E versus n is similar to what was developed for centro-symmetric Förster one-donor-multiple-acceptor assemblies such as QD-dye conjugates, $E_{FRET} = nR_0^6/(nR_0^6 + r^6)$, where R_0 is the Förster radius corresponding to $E_{FRET}(n=1) = 50\%$, and r is the center-to-center separation distance (see below).[43] Here K depends on the separation distance and β is related to the strength of the interactions between the QD and bound clusters. This analysis reflects two important features of our materials: (1) the centro-symmetric configuration of the QD-assemblies, imposed by the spherical nature of the QDs and the equidistant but random arrangement of the attached clusters; (2) the effects of heterogeneity in the conjugate

dx.doi.org/10.1021/jp404952x | J. Phys. Chem. C XXXX, XXX, XXX–XXX

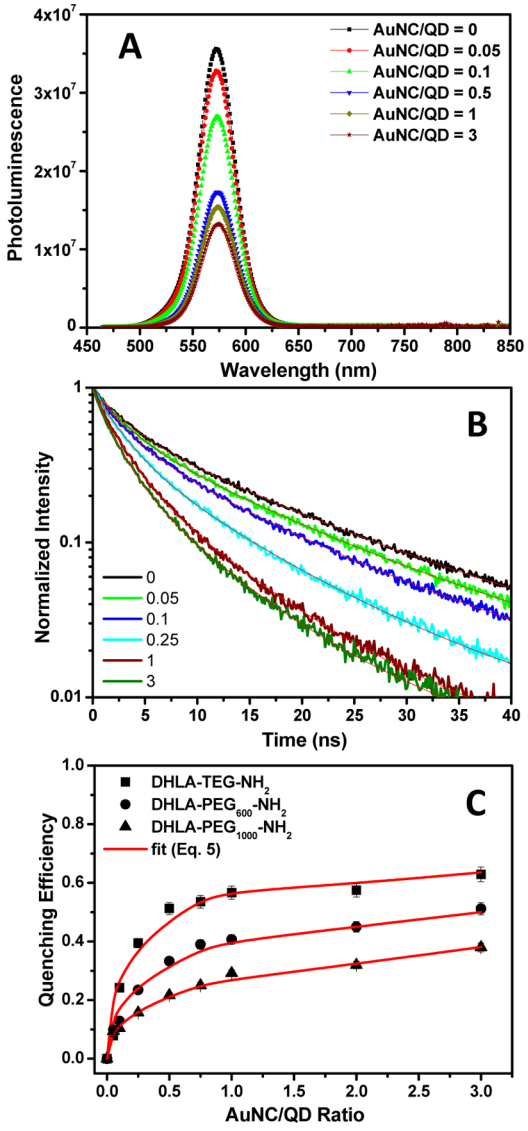

Figure 4. (A) Select PL spectra collected from 574-nm-emitting QD conjugates (formed using a PEG_{200}-plus-PEG_{600} bridge) after subtraction of the direct excitation contribution to the cluster emission and signal deconvolution (samples were excited at 450 nm); (B) the corresponding normalized time-resolved PL decay curves with increasing AuNC-to-QD ratio. (C) Cumulative plots of the quenching efficiency versus AuNC-to-QD molar ratio for conjugates using 574-nm-emitting QDs and three different PEG bridges, PEG_{200}-plus-PEG_{600} (square), PEG_{600}-plus-PEG_{600} (circle), and PEG_{1000}-plus-PEG_{600} (triangle). The solid red lines are fits to the data with the Poisson distribution correction taken into account (using eq 5).

structure (i.e., valence), which is an inherent property of these assemblies.[44,45]

The values for K/β extracted from fits by using eqs 5 and 6 vary with the size/emission of the QDs used (for QD-PEG-AuNCs conjugates with the same PEG_{600}-plus-PEG_{600} bridge), with K/β = 1.35, 3, and 8.2 for the green-, yellow-, and red-emitting QDs, respectively. The observed trend is consistent with the expected slight increase in K (due to an increase in the nanocrystal size) combined with a decrease in β due to changes in spectral overlap associated with red shifting of the QD emission. A similar trend is also observed when the separation distance between the QD and AuNCs is varied by using different PEG bridges while maintaining the same QDs in the assemblies: we measured K/β values of 1.8, 3, and 4.8 for assemblies using yellow-emitting QDs coupled via PEG_{200}-plus-PEG_{600}, PEG_{600}-plus-PEG_{600}, and PEG_{1000}-plus-PEG_{600} bridges, respectively (Figure 4).

We should note that fitting the experimental data (E vs n) by using only eq 6, without accounting for the heterogeneity in the conjugate valence (using the Poisson distribution), does not provide a good agreement with the experimental results (see Figure 2C). Moreover, the values for K/β extracted by using data fit to eq 6 are slightly different from (smaller than) those provided by fits to eq 5, with K/β = 0.39, 1.62, and 6.83 for the green-, yellow-, and red-emitting QDs, respectively. This is due to the fact that rather high quenching efficiencies are measured at low valences where conjugate heterogeneity plays a larger role.[44]

In the above treatment using E vs AuNC-to-QD molar ratio, we assumed that all the clusters have reacted with the QDs, producing a final valence equal to the molar ratios of added reactants. The data could also be analyzed by using a plot of E versus the concentration of the clusters (c_{AuNC}), using $E = \beta' c_{AuNC}/(\beta' c_{AuNC} + K)$, and a similar trend would result.[46] This is due to the fact that the final number of attached clusters per QD-conjugate is proportional to the relative concentrations of the QDs and clusters used during the coupling reaction, as anticipated from the first-order bimolecular kinetics.[47,48]

We would also like to emphasize that the quenching efficiencies measured for the present QD-AuNC assemblies are larger than what would be expected for QD-dye pairs having the same spectral overlap and dot-to-dye separation distance. For example, using the overlap integral measured for the 525-nm-emitting QD-AuNC pair ($I = 4.54 \times 10^{-13}$ cm^3 M^{-1}), the expected value for the Förster radius (given by $R_0 = [9.78 \times 10^3]\{n_D^{-4}\kappa_p^2\Phi_D I\}^{1/6}$ is ≅ 43 Å; here we used the QY of the QD (donor), Φ_D, the refractive index of the water medium, n_D, and a value for the dipole orientation parameter, k_p^2 = 2/3.[43,45] Combining the value for R_0, an estimate for the separation distance, r, extracted from the lateral extension of the PEG bridge r ≅ 55 Å, and the classical expression for the FRET efficiency given by $E = R_0^6/(R_0^6 + r^6)$, a quenching efficiency for a one-donor-to-one-acceptor pair of 0.20 is calculated.[24] We used a swollen (Flory type) configuration for the PEG bridge with a monomer size of 3.4 Å and an end-to-end-distance of ~2.3 nm.[49] This estimated quenching efficiency is 3 times smaller than that obtained for the equivalent QD-AuNC pair and is consistent with what we reported in our previous study.[27]

Our results also show that these QD-cluster systems exhibit another substantial difference from what is observed for a FRET process: there is no enhancement in the cluster fluorescence despite the substantial loss in the QD emission. Indeed, we consistently found that the contribution of the clusters to the measured PL spectra completely emanates from direct excitation, and once that direct excitation contribution is subtracted from the composite spectra, only the fraction of PL emission left from the QDs is collected for every set of QD-AuNC assemblies studied (see Figures 2–4). This is drastically different from what has been measured when fluorescent dyes (or proteins) are coupled to the QDs.[43,50] In those systems, the loss in QD PL is always accompanied with a substantial enhancement in the dye emission, unless the dye acceptor is a dark quencher.[24,51] Such enhancement was found to track the number of dyes coupled to a QD, and increases with increasing spectral overlap and/or decreasing separation distance. The

dx.doi.org/10.1021/jp404952x | J. Phys. Chem. C XXXX, XXX, XXX–XXX

data shown in Figures 2–4, though somewhat puzzling, indicate that the mechanism driving the interactions and quenching still shares a few common features with resonance energy transfer treated within the conventional Förster dipole–dipole interaction mechanism, with its reliance on proximity and spectral overlap. However, the absence of any enhancement in the cluster emission indicates that such quenching is driven by a process that is different from the conventional Förster dipole–dipole process, where the relaxation of QD excitation energy is altered nonradiatively and presumably lost into the surroundings as heat. No fraction of that excitation energy serves to resonantly excite the surrounding clusters and produce added contribution to their emission. We should note that additional experiments to measure the PLE (photoluminescence excitation or excitation scan) spectra of the clusters using detection anywhere across the emission profile consistently produced spectra that are similar in shape (see the Supporting Information, Figure S5). Furthermore, those spectra reproduced the features measured in the absorption profile shown in Figure 1. This essentially indicates that the fluorescence emission of these clusters obeys the Kasha rule.[52]

Radiative and Nonradiative Exciton Relaxation. To gain further insight into how the exciton relaxation pathways are affected/altered by the presence of the clusters, we follow the rationales we used in our previous report.[27] We introduce a nonradiative channel for the exciton relaxation (identified as energy transfer or energy loss), caused by interactions with the proximal clusters, with a decay rate k_{et}. As done previously, we assume that the QD PL nonradiative pathways (other than ET) are not affected by the cluster presence, i.e., $k_{nr} = k_{nr}^0$; k_{nr} and k_{nr}^0 correspond to QD-AuNC assemblies and QDs alone, respectively.[53,54] Using the expression of the QY as a function of the decay rates, one can derive relations between changes in the radiative and energy transfer rates, k_r and k_{et}, and the total decay rates, k^0 and k, of the QDs before and after assembly with the clusters.[25,27]

$$\frac{k_{et}}{k_r} = \left(\frac{1-\phi}{\phi}\right) - \left(\frac{1-\phi^0}{\phi}\right)\frac{k^0}{k} \tag{7}$$

$$\frac{k_r}{k_r^0} = \frac{\phi}{\phi^0}\frac{k_r + k_{nr} + k_{et}}{k_r^0 + k_{nr}^0} = \frac{\phi}{\phi^0}\frac{k}{k^0} \tag{8}$$

where Φ^0 and Φ are respectively the quantum yields (QY) measured in the absence and presence of AuNCs.

We use these expressions along with the experimental parameters to extract values for the energy transfer and radiative rates, k_{et} and k_r, as done in ref 27. Combining steady-state data and time-resolved QD PL measurements, we extracted estimates for the normalized radiative and energy transfer decay rates (using eqs 7 and 8) for the QD-AuNC conjugates, and tracked their dependence on the nanocrystal size (or spectral overlap). Table 1 shows the quenching efficiencies of the three sets of QDs used in this study after conjugation with approximately one AuNC per conjugate, along with the progression of k_r/k_r^0 and k_{et}/k_r. The ratio k_r/k_r^0 is equal to 0.67 ± 0.026, 0.83 ± 0.037, and 0.97 ± 0.04 for the green-, yellow-, and red-emitting QDs, respectively. Data show that the 525-nm-emitting QDs, which have the highest spectral overlap with the cluster absorption, exhibit the largest change (decrease) in the radiative rate compared to the control sample. Conversely, k_{et} is significantly higher ($k_{et}/k_r > 1$ for all three samples, see Table 1) and progressively decreases with increasing QD sizes, or decreasing spectral overlap. These observations confirm that while the QD radiative rate is slightly changed, the presence of AuNCs introduces a nonradiative pathway which importance strongly depends on the spectral overlap between QDs and Au clusters.

Similarly, Table 2 shows that the radiative decay rate, k_r, derived for the yellow-emitting QD-conjugates prepared by using PEG_{200}-plus-PEG_{600}, PEG_{600}-plus-PEG_{600}, or PEG_{1000}-plus-PEG_{600} bridges is essentially unchanged in the presence of AuNCs ($k_r/k_r^0 \approx 0.9$), even when the QD PL quenching is very efficient (shortest separation distance). However, the ratio k_{et}/k_r decreases with increasing separation distance (Table 2). This observation is similar to results reported in previous studies with dyes or QDs paired with AuNPs, and indicates that the ET decay rates are drastcially reduced at larger separation distances.[25,27]

Table 2. Summary of the PL Quenching Efficiencies Measured for 574 nm-emitting QDs Coupled to the AuNCs Using Three Different PEG Bridges.[a] The Corresponding Ratios k_r/k_r^0 and k_{et}/k_r are also Shown

	PEG_{200}-plus-PEG_{600} bridge	PEG_{600}-plus-PEG_{600} bridge	PEG_{1000}-plus-PEG_{600} bridge
PL quenching	0.57 ± 0.028	0.41 ± 0.022	0.27 ± 0.02
k_r/k_r^0	0.86 ± 0.03	0.83 ± 0.037	0.87 ± 0.046
k_{et}/k_r	6.65 ± 0.22	5.64 ± 0.49	3.14 ± 0.66

[a]Data compiled for an average QD-AuNC valence of 1.

Overall, the above results indicate that the radiative decay rates measured for the QD-AuNC conjugates with a fixed PEG bridge slightly increase with decreasing spectral overlap (Table 1). These rates are not affected by changes in the PEG bridge (separation distance) if the spectral overlap stays constant (e.g., see k_r/k_r^0 values for QD-AuNC conjugates assembled by using 574 nm-emitting QDs, Table 2). In contrast, k_{et} is significantly higher than k_r ($k_{et}/k_r > 1$) and progressively decreases with increasing separation distance. Decrease is even more pronounced with decreasing spectral overlap (see Table 1). These observations confirm that while the QD donor radiative rate is either marginally or not changed, the presence of the clusters introduces an additional and efficient nonradiative pathway for the QD exciton relaxation.[54] Nonetheless, the nonradiative interactions with the proximal Au clusters are "not resonant", as all the transferred excitation energy does not contribute additional enhancement to the emission of the AuNC "acceptors". This further confirms that the quenching of the QD emission in this system is controlled by quenching mechanisms other than the Förster resonant energy transfer process.

CONCLUSION

In summary, we have designed and tested a new energy transfer nanostructure model, combining luminescent CdSe-ZnS QDs and fluorescent gold nanoclusters (AuNCs). We used steady-state and time-resolved fluorescence measurements to systematically examine the quenching of the QD photoemission induced by interactions with the proximal AuNCs, and varied three important parameters: (1) the ratio of AuNC-to-QD for a given bridge length, (2) the spectral overlap using three different size QDs emitting at 525, 574, and 610 nm, and (3) the separation distance, using variable polyethylene glycol

dx.doi.org/10.1021/jp404952x | J. Phys. Chem. C XXXX, XXX, XXX–XXX

bridges. We found that higher quenching efficiency was measured for the smallest QD, which exhibits larger spectral overlap with the cluster absorption, and/or when shorter separation distances are used. We also found that, regardless of how strong the quenching for all QD samples studied was, no enhancement in the cluster emission was measured.

We attributed these findings to nonradiative alteration of the QD excitation energy due to interactions with the proximal metal clusters, where a strong energy transfer channel is introduced, while little to no change is measured for the radiative channel. Our results also indicate that the quenching of the QD fluorescence is due to mechanisms other than the conventional Förster (FRET) formalism. The strong quenching measured for these assemblies could provide an effective platform for sensing applications. In these constructs, a peptide or oligonucleotide bridge (e.g., recognized and cleaved by an enzyme) could be used to promote the interactions and quenching of the QD emission. The fixed cluster emission would provide a reference signal, while modulation of the QD emission will permit a quantification of the interaction efficiency and sensing.

■ ASSOCIATED CONTENT

Supporting Information

Additional data on the PL quenching from control solutions and using other QD-PEG-bridge-AuNC assemblies, along with PLE spectra collected from cluster dispersions. This material is available free of charge via the Internet at http://pubs.acs.org.

■ AUTHOR INFORMATION

Corresponding Author

* E-mail: mattoussi@chem.fsu.edu.

Notes

The authors declare no competing financial interest.

■ ACKNOWLEDGMENTS

We thank FSU and the National Science Foundation (NSF-CHE, No. 1058957) for financial support. We also thank Drs. Goutam Palui, Habeeb Muhammed and Thomas Pons (ESPCI Paris) for the helpful discussions.

■ REFERENCES

(1) Alivisatos, A. P.; Waldeck, D. H.; Harris, C. B. Nonclassical Behavior of Energy-Transfer from Molecules to Metal-Surfaces — Biacetyl(Normal-3-Pi-Star)/Ag(111). *J. Chem. Phys.* **1985**, *82*, 541–547.

(2) Dulkeith, E.; Morteani, A. C.; Niedereichholz, T.; Klar, T. A.; Feldmann, J.; Levi, S. A.; van Veggel, F. C.; Reinhoudt, D. N.; Moller, M.; Gittins, D. I. Fluorescence Quenching of Dye Molecules near Gold Nanoparticles: Radiative and Nonradiative Effects. *Phys. Rev. Lett.* **2002**, *89*, 203002.

(3) Haldar, K. K.; Sen, T.; Patra, A. Au@ZnO Core-Shell Nanoparticles are Efficient Energy Acceptors with Organic Dye Donors. *J. Phys. Chem. C* **2008**, *112*, 11650–11656.

(4) Burda, C.; Chen, X. B.; Narayanan, R.; El-Sayed, M. A. Chemistry and Properties of Nanocrystals of Different Shapes. *Chem. Rev.* **2005**, *105*, 1025–1102.

(5) Mayilo, S.; Kloster, M. A.; Wunderlich, M.; Lutich, A.; Klar, T. A.; Nichtl, A.; Kurzinger, K.; Stefani, F. D.; Feldmann, J. Long-Range Fluorescence Quenching by Gold Nanoparticles in a Sandwich Immunoassay for Cardiac Troponin T. *Nano Lett* **2009**, *9*, 4558–4563.

(6) Acuna, G. P.; Bucher, M.; Stein, I. H.; Steinhauer, C.; Kuzyk, A.; Holzmeister, P.; Schreiber, R.; Moroz, A.; Stefani, F. D.; Liedl, T.; Simmel, F. C.; Tinnefeld, P. Distance Dependence of Single-Fluorophore Quenching by Gold Nanoparticles Studied on DNA Origami. *ACS Nano* **2012**, *6*, 3189–3195.

(7) De, M.; Ghosh, P. S.; Rotello, V. M. Applications of Nanoparticles in Biology. *Adv. Mater.* **2008**, *20*, 4225–4241.

(8) Griffin, J.; Singh, A. K.; Senapati, D.; Rhodes, P.; Mitchell, K.; Robinson, B.; Yu, E.; Ray, P. C. Size- and Distance-Dependent Nanoparticle Surface-Energy Transfer (NSET) Method for Selective Sensing of Hepatitis C Virus RNA. *Chem.—Eur. J.* **2009**, *15*, 342–351.

(9) Sen, T.; Patra, A. Recent Advances in Energy Transfer Processes in Gold-Nanoparticle-Based Assemblies. *J. Phys. Chem. C* **2012**, *116*, 17307–17317.

(10) Singh, M. P.; Strouse, G. F. Involvement of the LSPR Spectral Overlap for Energy Transfer between a Dye and Au Nanoparticle. *J. Am. Chem. Soc.* **2010**, *132*, 9383–9391.

(11) Gueroui, Z.; Libchaber, A. Single-Molecule Measurements of Gold-Quenched Quantum Dots. *Phys. Rev. Lett.* **2004**, *93*, 166108–166111.

(12) Medintz, I. L.; Pons, T.; Trammell, S. A.; Grimes, A. F.; English, D. S.; Blanco-Canosa, J. B.; Dawson, P. E.; Mattoussi, H. Interactions between Redox Complexes and Semiconductor Quantum Dots Coupled via a Peptide Bridge. *J. Am. Chem. Soc.* **2008**, *130*, 16745–16756.

(13) Nikoobakht, B.; Burda, C.; Braun, M.; Hun, M.; El-Sayed, M. A. The Quenching of CdSe Quantum Dots Photoluminescence by Gold Nanoparticles in Solution. *Photochem. Photobiol.* **2002**, *75*, 591–7.

(14) Oh, E.; Hong, M. Y.; Lee, D.; Nam, S. H.; Yoon, H. C.; Kim, H. S. Inhibition Assay of Biomolecules Based on Fluorescence Resonance Energy Transfer (FRET) between Quantum Dots and Gold Nanoparticles. *J. Am. Chem. Soc.* **2005**, *127*, 3270–3271.

(15) Oh, E.; Susumu, K.; Goswami, R.; Mattoussi, H. One-Phase Synthesis of Water-Soluble Gold Nanoparticles with Control over Size and Surface Functionalities. *Langmuir* **2010**, *26*, 7604–7613.

(16) Mattoussi, H.; Palui, G.; Na, H. B. Luminescent Quantum Dots as Platforms for Probing in vitro and in vivo Biological Processes. *Adv. Drug Deliver Rev.* **2012**, *64*, 138–166.

(17) Michalet, X.; Pinaud, F.; Bentolila, L.; Tsay, J.; Doose, S.; Li, J.; Sundaresan, G.; Wu, A.; Gambhir, S.; Weiss, S. Quantum Dots for Live Cells, In Vivo Imaging, and Diagnostics. *Science* **2005**, *307*, 538–544.

(18) Gersten, J. I.; Nitzan, A. Photophysics and Photochemistry near Surfaces and Small Particles. *Surf. Sci.* **1985**, *158*, 165–189.

(19) Li, M.; Cushing, S. K.; Wang, Q. Y.; Shi, X. D.; Hornak, L. A.; Hong, Z. L.; Wu, N. Q. Size-Dependent Energy Transfer between CdSe/ZnS Quantum Dots and Gold Nanoparticles. *J. Phys. Chem. Lett.* **2011**, *2*, 2125–2129.

(20) Mandal, G.; Bardhan, M.; Ganguly, T. Occurrence of Forster Resonance Energy Transfer between Quantum Dots and Gold Nanoparticles in the Presence of a Biomolecule. *J. Phys. Chem. C* **2011**, *115*, 20840–20848.

(21) Lee, H.; Kim, A.; Kang, T.; Joo, S.-W.; Lee, S. Y.; Yoon, K.-A.; Lee, K. Selective Energy Transfer Between Quantum Dots and Gold Nanoparticles for Detection of Multiple Mutations in Epidermal Growth Factor Receptor. *Anal. Lett.* **2012**, *45*, 2707–2716.

(22) Yang, D. Z.; Xu, S. K.; Chen, Q. F.; Wang, Y. One System with two Fluorescence Resonance Energy Transfer (FRET) Assembles Among Quantum Dots, Gold Nanoparticles and Enzyme. *Colloid Surf., A* **2008**, *329*, 38–43.

(23) Choi, Y.; Cho, Y.; Kim, M.; Grailhe, R.; Song, R. Fluorogenic Quantum Dot-Gold Nanoparticle Assembly for Beta Secretase Inhibitor Screening in Live Cell. *Anal. Chem.* **2012**, *84*, 8595–601.

(24) Lakowicz, J. R. *Principles of Fluorescence Spectroscopy*, 3rd ed.; Springer: New York, NY, 2006; p 954.

(25) Jennings, T. L.; Singh, M. P.; Strouse, G. F. Fluorescent Fifetime Quenching near d = 1.5 nm Gold Nanoparticles: Probing NSET Validity. *J. Am. Chem. Soc.* **2006**, *128*, 5462–7.

(26) Yun, C. S.; Javier, A.; Jennings, T.; Fisher, M.; Hira, S.; Peterson, S.; Hopkins, B.; Reich, N. O.; Strouse, G. F. Nanometal Surface Energy Transfer in Optical Rulers, Breaking the FRET Barrier. *J. Am. Chem. Soc.* **2005**, *127*, 3115–3119.

(27) Pons, T.; Medintz, I. L.; Sapsford, K. E.; Higashiya, S.; Grimes, A. F.; English, D. S.; Mattoussi, H. On the Quenching of Semiconductor Quantum Dot Photoluminescence by Proximal Gold Nanoparticles. *Nano Lett* **2007**, *7*, 3157−3164.
(28) Shang, L.; Dong, S. J.; Nienhaus, G. U. Ultra-small fluorescent metal nanoclusters: Synthesis and biological applications. *Nano Today* **2011**, *6*, 401−418.
(29) Muhammed, M. A. H.; Verma, P. K.; Pal, S. K.; Retnakumari, A.; Koyakutty, M.; Nair, S.; Pradeep, T. Luminescent Quantum Clusters of Gold in Bulk by Albumin-Induced Core Etching of Nanoparticles: Metal Ion Sensing, Metal-Enhanced Luminescence, and Biolabeling. *Chem.—Eur. J.* **2010**, *16*, 10103−10112.
(30) Jin, R. C. Quantum Sized, Thiolate-Protected Gold Nanoclusters. *Nanoscale* **2010**, *2*, 343−362.
(31) Lin, C. A. J.; Lee, C. H.; Hsieh, J. T.; Wang, H. H.; Li, J. K.; Shen, J. L.; Chan, W. H.; Yeh, H. I.; Chang, W. H. Synthesis of Fluorescent Metallic Nanoclusters toward Biomedical Application: Recent Progress and Present Challenges. *J. Med. Biol. Eng.* **2009**, *29*, 276−283.
(32) Zheng, J.; Zhang, C. W.; Dickson, R. M. Highly Fluorescent, Water-soluble, Size-Tunable Gold Quantum Dots. *Phys. Rev. Lett.* **2004**, *93*, 077402.
(33) Zheng, J.; Nicovich, P. R.; Dickson, R. M. Highly Fluorescent Noble-Metal Quantum Dots. *Annu. Rev. Phys. Chem.* **2007**, *58*, 409−431.
(34) Muhammed, M. A.; Aldeek, F.; Palui, G.; Trapiella-Alfonso, L.; Mattoussi, H. Growth of in situ Functionalized Luminescent Silver Nanoclusters by Direct Reduction and Size Focusing. *ACS Nano* **2012**, *6*, 8950−8961.
(35) Aldeek, F.; Muhammed, M. A. H.; Palui, G.; Zhan, N. Q.; Mattoussi, H. Growth of Highly Fluorescent Polyethylene Glycol- and Zwitterion-Functionalized Gold Nanoclusters. *ACS Nano* **2013**, *7*, 2509−2521.
(36) Mei, B. C.; Susumu, K.; Medintz, I. L.; Mattoussi, H. Polyethylene Glycol-Based Bidentate Ligands to Enhance Quantum Dot and Gold Nanoparticle Stability in Biological Media. *Nat. Protoc.* **2009**, *4*, 412−423.
(37) Susumu, K.; Mei, B. C.; Mattoussi, H. Multifunctional Ligands Based on Dihydrolipoic Acid and Polyethylene Glycol to Promote Biocompatibility of Quantum Dots. *Nat. Protoc.* **2009**, *4*, 424−436.
(38) Murray, C. B.; Norris, D. J.; Bawendi, M. G. Synthesis and Characterization of Nearly Monodisperse Cde (E = S, Se, Te) Semiconductor Nanocrystallites. *J. Am. Chem. Soc.* **1993**, *115*, 8706−8715.
(39) Reiss, P.; Protiere, M.; Li, L. Core/Shell Semiconductor Nanocrystals. *Small* **2009**, *5*, 154−168.
(40) Hines, M. A.; Guyot-Sionnest, P. Synthesis and Characterization of Strongly Luminescing ZnS-Capped CdSe Nanocrystals. *J. Phys. Chem.* **1996**, *100*, 468−471.
(41) Dabbousi, B. O.; RodriguezViejo, J.; Mikulec, F. V.; Heine, J. R.; Mattoussi, H.; Ober, R.; Jensen, K. F.; Bawendi, M. G. (CdSe)ZnS Core-Shell Quantum Dots: Synthesis and Characterization of a Size Series of Highly Luminescent Nanocrystallites. *J. Phys. Chem. B* **1997**, *101*, 9463−9475.
(42) Mattoussi, H.; Cumming, A. W.; Murray, C. B.; Bawendi, M. G.; Ober, R. Properties of CdSe Nanocrystal Dispersions in the Dilute Regime: Structure and Interparticle Interactions. *Phys. Rev. B* **1998**, *58*, 7850−7863.
(43) Clapp, A. R.; Medintz, I. L.; Mauro, J. M.; Fisher, B. R.; Bawendi, M. G.; Mattoussi, H. Fluorescence Resonance Energy Transfer between Quantum Dot Donors and Dye-labeled Protein Acceptors. *J. Am. Chem. Soc.* **2004**, *126*, 301−310.
(44) Pons, T.; Medintz, I. L.; Wang, X.; English, D. S.; Mattoussi, H. Solution-Phase Single Quantum Dot fluorescence Resonance Energy Transfer. *J. Am. Chem. Soc.* **2006**, *128*, 15324−15331.
(45) Medintz, I. L.; Mattoussi, H. Quantum Dot-Based Resonance Energy Transfer and its Growing Application in Biology. *Phys. Chem. Chem. Phys.* **2009**, *11*, 17−45.
(46) Ji, X.; Palui, G.; Avellini, T.; Na, H. B.; Yi, C.; Knappenberger, K. L.; Mattoussi, H. On the pH-Dependent Quenching of Quantum Dot Photoluminescence by Redox Active Dopamine. *J. Am. Chem. Soc.* **2012**, *134*, 6006−6017.
(47) Vijayendran, R. A.; Ligler, F. S.; Leckband, D. E. A Computational Reaction-Diffusion Model for the Analysis of Transport-Limited Kinetics. *Anal. Chem.* **1999**, *71*, 5405−5412.
(48) Sapsford, K. E.; Pons, T.; Medintz, I. L.; Higashiya, S.; Brunel, F. M.; Dawson, P. E.; Mattoussi, H. Kinetics of Metal-Affinity Driven Self-Assembly between Proteins or Peptides and CdSe-ZnS Quantum Dots. *J. Phys. Chem. C* **2007**, *111*, 11528−11538.
(49) Lee, H.; Venable, R. M.; MacKerell, A. D., Jr.; Pastor, R. W. Molecular Dynamics Studies of Polyethylene Oxide and Polyethylene Glycol: Hydrodynamic Radius and Shape Anisotropy. *Biophys. J.* **2008**, *95*, 1590−1599.
(50) Dennis, A. M.; Bao, G. Quantum Dot−Fluorescent Protein Pairs as Novel Fluorescence Resonance Energy Transfer Probes. *Nano Lett.* **2008**, *8*, 1439−1445.
(51) Medintz, I. L.; Clapp, A. R.; Mattoussi, H.; Goldman, E. R.; Fisher, B.; Mauro, J. M. Self-assembled Nanoscale Biosensors Based on Quantum Dot FRET Donors. *Nat. Mater.* **2003**, *2*, 630−638.
(52) Kasha, M. Characterization of Electronic Transitions in Complex Molecules. *Discuss. Faraday Soc.* **1950**, *9*, 14−19.
(53) Schlegel, G.; Bohnenberger, J.; Potapova, I.; Mews, A. Fluorescence Decay Time of Single Semiconductor Nanocrystals. *Phys. Rev. Lett.* **2002**, *88*, 37401.
(54) Carminati, R.; Greffet, J. J.; Henkel, C.; Vigoureux, J. M. Radiative and Non-radiative Decay of a Single Molecule Close to a Metallic Nanoparticle. *Opt. Commun.* **2006**, *261*, 368−375.